Iron ore sinter in the analytical transmission electron microscope

R. MULVANEY

Department of Metallurgy, University of Sheffield, Mappin Street, Sheffield, S1 3JD*

Abstract

Iron ore sinters prepared for the blast furnaces at Scunthorpe, Humberside, comprise iron oxides bound in a matrix of aluminium- and silicon-rich calcium ferrites with some calcium orthosilicate and a residual silicate glass. A super-silicon-deficient clinopyroxene with up to half of the Si in the chain replaced by Fe^{3+} and Al^{3+} precipitates from the glass in some areas. The iron oxides are principally magnetite and hematite with some wüstite in highly reduced areas. The calcium orthosilicate has been previously reported as the mineral larnite, β-Ca_2SiO_4. This study found a range of Fe for Ca substitution and three polymorphs were recognised: the range Ca_2SiO_4 to $Ca_{1.85}Fe_{0.15}SiO_4$ has the structure of larnite; the range $Ca_{1.85}Fe_{0.15}SiO_4$ to $Ca_{1.6}Fe_{0.4}SiO_4$ has the structure of bredigite, α'-Ca_2SiO_4. Iron substitution beyond this, and up to a maximum of about $Ca_{1.5}Fe_{0.5}SiO_4$, was not recognisable as a polymorph of Ca_2SiO_4, but an orthorhombic cell is tentatively proposed. The complex ferrite SFCA (silico-ferrite of Ca and Al) is variable in composition, but has a minimum of about 3 wt. % Al_2O_3 and contains 20 wt. % CaO and SiO_2 with a Ca : Si ion ratio of about 2 : 1. A *C*-face centred monoclinic cell has been deduced: *a* 15.70, *b* 9.70, *c* 8.48 Å; β 105°30′. The Al appears critical for the formation of SFCA in sinter; without it, a eutectic of magnetite and bredigite precipitates in preference.

KEYWORDS: iron ore sinters, electron microscopy, ferrites.

Introduction

As much as 95% of the world's iron is produced by the blast furnace process and is the basis for most primary steelmaking. Scott *et al.* (1986) described the mineralogy of blast furnace slags, the major waste product of iron making. This paper describes some of the mineralogy of iron ore sinters, the main raw material for many blast furnaces.

Historically, the blast furnace burden tended to be run-of-mine lump iron ore, coke fuel and fluxes, such as limestone, charged directly to the furnace with little or no preparation. However, the modern basic oxygen steelmaking process demands large quantities of hot iron of consistent composition. This in turn demands a blast furnace burden of consistent quality. Iron ore sinter satisfies this criterion and now constitutes the major iron-bearing component charged to the blast furnace.

Sinter is produced from a mixture of crushed iron ore, usually from several sources; fluxes, mainly limestone but may include dolomite, olivine or sand; and a fuel, usually coke breeze. The mixture is blended, moistened, fed onto a moving grate to a depth of about 40 cm and the surface ignited. An air blast drawn down through the bed propagates a heat wave through the material causing it to melt at the wave front. Most of the mixture is assimilated by the liquid and a series of reactions take place as the temperature rapidly rises to a maximum of about 1250–1350 °C. After the heat wave has passed, the material quickly cools under the influence of the down draught to near ambient temperature in 10–20 minutes. The sinter is then broken up, graded and fed to the blast furnace.

The texture of sinter shows a highly porous, heterogeneous array of relict and exsolved magnetite and hematite, with occasionally some wüstite, bonded by either a matrix of silicates and silicate-rich glasses, or by a matrix of calcium ferrite minerals with some interstitial calcium silicate. The main criterion governing which matrix occurs is the ratio CaO/SiO_2 in the sinter mix. In self-fluxed sinters this ratio will be set at about 1.1 to 1.5 and the matrix will be glassy (Fig. 1A). In super-fluxed sinter, a ratio of between 1.5 to 2.5 will give a matrix

* Present address: British Antarctic Survey, High Cross, Madingley Road, Cambridge, CB3 0ET.

Mineralogical Magazine, March 1987, Vol. 51, pp. 61–9

of calcium ferrite which may achieve 50% of sinter bulk (Fig. 1B). A lime-silica ratio above 2.5 is rare in commercial plant sinter.

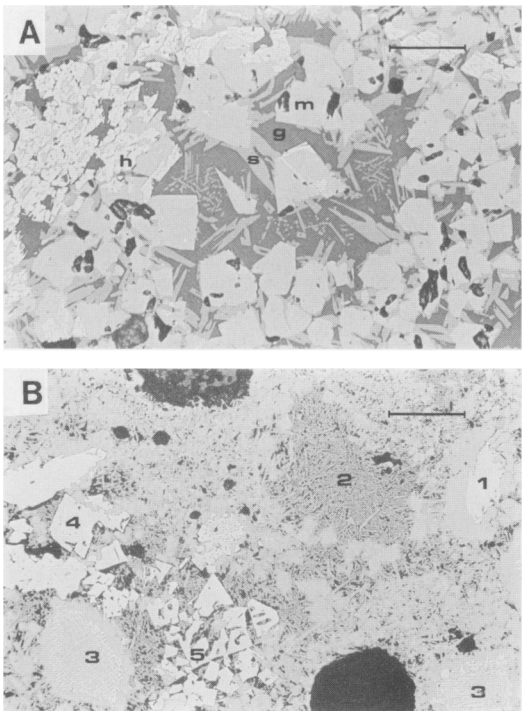

FIG. 1. Reflected-light micrographs of iron ore sinter. (A) A typical, self-fluxed sinter: specimen 6548, with a lime/silica ratio of 1.24. Euhedral to subhedral exsolved magnetite (m) and hematite (h) set in partially devitrified glass (g), with some lath-shaped calcium ferrite of the SFCA type (s). (B) A typical, super-fluxed sinter: specimen 7296, with a lime/silica ratio of 1.72. 1, relict hematite grain surrounded by exsolved magnetite; 2, region of needle-shaped SFCA crystals with interstitial calcium orthosilicate; 3, exsolved magnetite grains showing subsequent reoxidation lamellae of hematite; 4, relic hematite surrounded by exsolved hematite; 5, area of subhedral hematite grains. The dark circular areas are pores in the sinter. Scale bars 0.1 mm.

A suite of 12 experimental and plant sinters of variable composition was supplied by the British Steel Corporation, Scunthorpe Division for analysis. Their bulk chemistry and mineralogy is given in Tables 1 and 2, which show the dependence of the matrix components on the lime/silica ratio. The very fine-grained texture of sinter makes its study by analytical transmission electron microscope (ATEM) techniques particularly appropriate.

Technique

The sinter mineralogy described here was observed in a Philips EM400T transmission electron microscope operating at an acceleration voltage of 100 kV. Electron-transparent specimens were prepared by ion-beam thinning small areas of interest from 30 μm thick petrological slides, mounted on 3 mm diameter copper support discs, using a Gatan model 600 Dual Ion Mill.

Thin-specimen microprobe analyses were obtained with the Philips EM400T equipped with an EDAX 9100/60 energy-dispersive X-ray analysis system. The specimen was surrounded by a beryllium insert to reduce background X-ray generation

Table 1. Bulk XRF analyses of sinter specimens, with oxide concentrations corrected for ferrous iron using results from standard, wet-chemical determinations.

Sample	6249	6433	6468	6524	6548	6963
Na_2O %	0.16	0.26	0.32	0.04	0.14	0.22
MgO	1.94	1.34	1.12	0.98	0.84	1.10
Al_2O_3	2.74	2.26	2.68	2.48	2.40	3.88
SiO_2	8.46	9.76	7.44	9.06	8.74	6.44
P_2O_5	0.48	0.38	0.44	0.52	0.40	0.48
S	0.02	0.02	0.02	0.02	0.04	0.02
K_2O	0.18	0.18	0.18	0.18	0.20	0.18
CaO	10.04	9.64	8.94	9.92	10.88	9.72
TiO_2	0.18	0.14	0.13	0.26	0.25	0.15
MnO	0.60	0.58	0.58	0.54	0.58	0.60
FeO	36.60	16.70	14.90	17.20	31.80	10.41
Fe_2O_3	38.79	58.76	64.86	59.50	43.39	67.99
Total	100.19	100.02	101.61	100.70	99.66	101.17
CaO/SiO_2	1.19	0.99	1.20	1.09	1.24	1.51
Sample	**7093**	**7272**	**7296**	**7300**	**7302**	**7306**
Na_2O %	0.14	0.14	0.20	0.24	0.12	0.06
MgO	2.10	1.58	1.48	1.94	1.46	1.46
Al_2O_3	2.30	3.60	2.84	1.58	1.68	1.82
SiO_2	8.18	7.52	7.94	7.88	7.48	7.52
P_2O_5	0.34	0.54	0.60	0.32	0.30	0.32
S	0.02	0.06	0.02	0.04	0.02	0.02
K_2O	0.16	0.20	0.18	0.18	0.18	0.18
CaO	8.68	15.30	13.66	12.68	14.12	14.54
TiO_2	0.20	0.17	0.16	0.16	0.17	0.18
MnO	0.58	0.70	0.66	0.30	0.34	0.34
FeO	17.58	9.54	8.74	16.10	17.06	17.06
Fe_2O_3	60.30	61.34	64.27	58.53	55.54	54.61
Total	100.58	100.69	100.75	99.95	98.47	98.65
CaO/SiO_2	1.06	2.03	1.72	1.61	1.89	1.93

during analysis. Element concentrations were derived from characteristic X-ray intensities using the technique of scaling factors or k-values developed by Cliff and Lorimer (1975). A series of k-values for the elements of interest was obtained for this microscope initially by Ireland (1982) and refined whenever possible.

Table 2. Bulk mineralogy of sinter specimens, determined by standard, point-counting techniques in the reflected light microscope.

Sample		6249	6433	6468	6524	6548	6963
H1	%	1.8	0.8	9.2	1.6	1.0	3.4
H2		2.4	13.0	10.8	9.6	1.8	14.2
H3		0.4	0.8	1.2	0.2	0.2	0.0
M		55.8	52.8	53.6	54.6	53.4	47.2
W		10.6	0.4	0.4	1.2	8.4	0.0
SFCA		2.6	4.2	7.4	4.6	2.6	19.2
Glass		25.2	26.0	13.6	26.4	27.8	12.4
C2S		1.2	1.2	1.2	0.4	4.2	2.6
Pyr		0.0	0.8	1.6	1.2	0.4	1.0

Sample		7093	7272	7296	7300	7302	7306
H1	%	4.2	3.6	6.0	2.4	0.8	3.2
H2		6.4	5.6	8.4	14.4	13.2	8.0
H3		1.2	0.0	0.0	1.6	0.8	1.2
M		57.0	32.4	24.4	35.6	43.6	42.0
W		0.0	0.0	0.0	0.0	0.4	1.6
SFCA		4.6	44.0	48.0	22.0	20.8	27.2
Glass		27.4	10.8	8.8	14.0	16.0	10.4
C2S		0.4	3.6	4.8	9.8	4.8	7.6
Pyr		1.8	0.0	0.0	0.2	0.4	0.4

Explanation of symbols:-

H1 - relict hematite
H2 - hematite exsolved from the melt
H3 - reoridised hematite lamellae
M - exsolved magnetite
W - wustite
SFCA - silico-ferrite of calcium and aluminium
Glass - vitrified and partially devitrified silicate glass
C2S - calcium orthosilicate
Pyr - pyroxene-like mineral

Calcium orthosilicate

β-calcium orthosilicate or larnite (β-Ca_2SiO_4), has long been known to occur in sinter (Nyquist, 1962; Mazanek and Jasienska, 1968). It appears as small, lenticular grains, usually co-precipitated with calcium ferrite. β-calcium orthosilicate is thermodynamically unstable below 675 °C and may invert to the stable γ-calcium orthosilicates (Bredig, 1950). This inversion proceeds with an approximate 10% volume increase which was shown by Rankin and Wright (1915) to lead to a shattering of the phase to a fine powder. Although larnite rarely exceeds a small part of the matrix, this phase transformation is thought to be a cause of structural weakness in sinter. However, Zerfoss and Davis (1943) have shown that the β-γ inversion can be prevented by the addition of small quantities of oxides to the silicate melt prior to crystallisation of the calcium silicate, a situation common in the sinter silicate melt.

It was immediately apparent from single crystal analyses in the ATEM that the calcium orthosilicate was neither pure Ca_2SiO_4 nor of a single crystallographic form. Up to 24 wt. % FeO was present in the orthosilicate analyses together with small amounts of MgO, Al_2O_3 and P_2O_5. (As the oxidation state of the iron was unobtainable, it was assumed to be ferrous to allow isomorphic replacement of Ca^{2+}. This is to some extent justified by Bowen *et al.*, 1933, who showed that the level of Fe_2O_3 does not exceed 2 wt. % in the system Ca_2SiO_4–Fe_2SiO_4). Three distinct crystallographic forms of calcium orthosilicate were found depending on the degree of Fe for Ca substitution.

For comparison, a specimen of natural larnite from the dolerite–limestone contact at Scawt Hill, Larne, Northern Ireland (described by Tilley and Vincent, 1933) was prepared for the ATEM. Analysis showed this to be almost pure Ca_2SiO_4 (Table 3) and diffraction patterns from a number of zones consistently indexed on the unit cell of

Table 3. TEM analyses of some sinter minerals.

Mineral		A	B	C	D	E	F	G
MgO	%	nd	nd	nd	1.69	2.19	0.61(0.25)	0.42(0.32)
Al_2O_3		0.49	0.88	0.97	0.89	1.10	6.90(0.51)	4.87(1.16)
SiO_2		34.13	33.60	32.93	31.05	31.07	25.39(1.84)	7.25(1.94)
P_2O_5		0.79	2.08	2.11	1.14	1.21	1.00(0.14)	0.43(0.26)
K_2O		0.37	0.65	0.40	0.39	0.74	0.20(0.06)	0.07(0.09)
CaO		63.71	61.20	58.39	53.46	44.79	22.11(1.00)	14.02(2.51)
TiO_2		nd	nd	nd	nd	nd	0.54(0.09)	0.21(0.20)
MnO		0.03	nd	0.12	nd	0.43	0.47(0.10)	0.40(0.13)
FeO		0.48	1.59	5.08	11.38	18.47	0	0
Fe_2O_3		0	0	0	0	0	42.79(2.12)	74.83(4.83)
					FORMULAE			
Mg		....	....	....	0.07	0.10	0.04	0.20
Al		0.02	0.03	0.03	0.03	0.04	0.35	1.84
Si		0.98	0.96	0.95	0.92	0.93	1.09	2.31
P		0.02	0.05	0.05	0.03	0.03	0.04	0.11
K		0.01	....	0.01	0.02	0.03	0.01	0.03
Ca		1.95	1.87	1.80	1.69	1.43	1.02	4.81
Ti		....	....	....	....	....	0.02	0.05
Mn		....	....	....	....	0.01	0.02	0.11
Fe^{2+}		0.01	0.04	0.12	0.28	0.46	0	0
Fe^{3+}		0	0	0	0	0	1.39	18.06
Oxygen		4	4	4	4	4	6	40

A - natural larnite specimen from Scawt Hill
B - pure calcium orthosilicate, indexed as larnite
C - low-iron calcium orthosilicate, indexed as larnite
D - medium-iron calcium orthosilicate, indexed as bredigite
E - high-iron calcium orthosilicate, tentatively indexed with an orthorhombic cell
F - pyroxene-like mineral, mean of 21 single crystal analyses (standard deviation in brackets)
G - silico-ferrite of calcium and aluminium (SFCA), mean of 45 single crystal analyses (standard deviation in brackets)

β-Ca_2SiO_4, the medium–low temperature polymorph of calcium orthosilicate: monoclinic; *a* 5.507, *b* 6.754, *c* 9.317 Å; β 94° 37′ (JCPDS index, card 9-351). This mineral showed a strong preference to multiple, lamellar twinning of regular periodicity, parallel to the (100) plane (Fig. 2A).

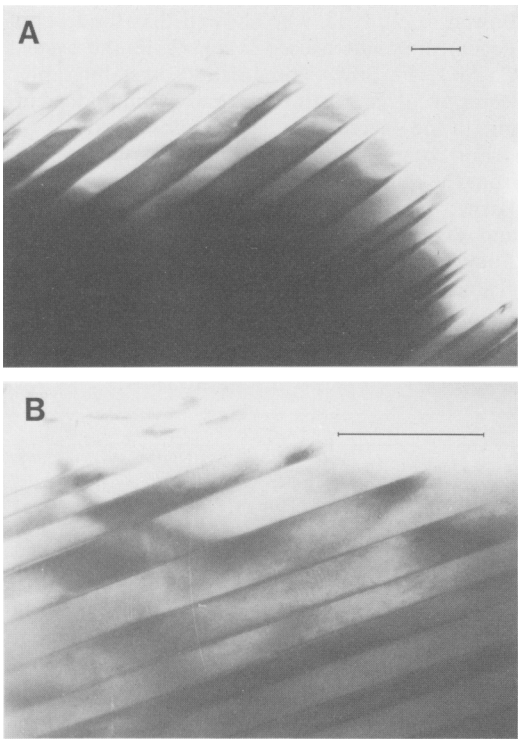

FIG. 2. TEM micrographs of the regular, (100) twinning of the mineral larnite. (A) An example of the natural mineral taken from the dolerite-limestone contact at Scawt Hill, Larne, Northern Ireland. Scale bar 1 μm. (B) The sinter larnite (the low-iron calcium orthosilicate) shows the (100) twinning on a finer scale. Scale bar 0.5 μm.

This characteristic twinning was evident in many of the calcium orthosilicate crystals present in sinter (Fig. 2B), though on a finer scale (approximately 1μm between successive twins in the natural larnite compared to 0·2 μm for sinter). This probably reflects the faster cooling regime present on the sinter production strand. Analyses of the twinned examples showed them to be consistently low in iron, up to an approximate maximum corresponding to $(Ca_{1.85}Fe_{0.15})SiO_4$. Diffraction patterns indicated that these silicates have the same crystallography as the natural larnite and the twinning is in the same manner, parallel to (100). An example is given in Fig. 3A.

As Fe replaced Ca in the analyses of the orthosilicate the distinctive twinning was lost and diffraction patterns (e.g. Fig. 3B) were no longer consistent with larnite, but were readily indexed on the unit cell of bredigite, the medium–high temperature form of calcium orthosilicate, α'-Ca_2SiO_4: orthorhombic; *a* 10.91, *b* 18.41, *c* 6.76 Å (taken from Bridge, 1966). For this phase, the analyses gave approximately $(Ca_{1.7}Fe_{0.3})SiO_4$ (Table 3).

At the upper end of the observed range of Fe for Ca substitution, represented by an apparent limit $(Ca_{1.5}Fe_{0.5})SiO_4$, diffraction patterns (e.g. Fig. 3C) were not consistent with either larnite or bredigite. There were certain similarities with diffraction patterns obtained from larnite, though the symmetry suggested an orthorhombic cell. Midgley (1952), in her description of the crystal structure of larnite, noted that the Si and Ca atoms lie close to the $x = 1/4$ planes and require only a slight shift and a small rotation, the β angle being reduced from 94° 37′ to 90°, to produce orthorhombic symmetry. Acting on this information, an orthorhombic cell was deduced; *a* 5.32, *b* 6.81, *c* 9.17 Å; this cell proved adequate to describe most of the high iron calcium orthosilicate diffraction patterns. However, this cell is speculative; further work may show it to be incorrect.

These results should be compared with the phase diagram for the Ca_2SiO_4–Fe_2SiO_4 binary described by Bowen *et al.* (1933). They note a solid solution of iron in β-Ca_2SiO_4 to a limit of 10 wt. % Fe_2SiO_4 at 1230 °C (i.e. at about the temperature attained on the sinter strand). This corresponds well with the Fe–Ca replacement which was shown above to give the multiply twinned larnite. With increased Fe_2SiO_4 Bowen found no further Fe for Ca substitution, but rather that β-Ca_2SiO_4 solid solutions are formed in coexistence with Ca–Fe olivines. The present study found no evidence of any olivine but that further Fe substitution is possible with a structural change to that of α'-calcium orthosilicate, bredigite. Bowen suggests that the Fe-olivine, Fe_2SiO_4, is capable of accepting a greater range of Ca for Fe replacement up to a limit corresponding to approximately $Ca_{1.2}Fe_{0.8}SiO_4$ (later confirmed by Wyderko and Mazanek, 1968). This limit of Ca in the olivine structure does not extend into the range of Ca–Fe silicates found in this study. It seems unlikely then that these sinter silicates are substituted olivines and indeed no diffraction data were obtained which could have indicated an olivine structure.

In conclusion, it appears that the binary diagram of Bowen *et al.* (1933) does not explain the phase relationships found for the Ca–Fe silicates found in

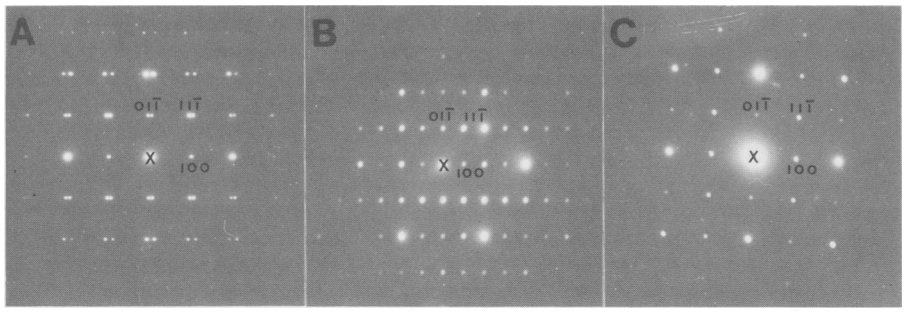

FIG. 3. The [011] zone electron diffraction patterns taken from the three polymorphs of iron calcium orthosilicate. (A) Low-iron calcium orthosilicate. The unit cell is the *C*-face centred monoclinic cell of larnite. The twinning is evident in this pattern. (B) Medium-iron calcium orthosilicate. The unit cell is the orthorhombic cell of bredigite. (C) High-iron calcium orthosilicate. The unit cell is primitive orthorhombic.

sinter. A binary phase diagram linking calcium orthosilicate with iron oxide, which may include the Fe-rich calcium silicate, could not be found.

Pyroxene-like phase

A mineral crystallising from glass with a characteristic dendritic habit occurs widely in self-fluxed sinters (Fig. 4A), though it rarely makes up more than 1–2 vol. % of the sinter bulk. The identity of this phase is open to some speculation. It was for many years considered to be a member of the melilite series close to gehlenite (McBriar *et al.*, 1954) and was apparently confirmed later as iron gehlenite $Ca_2Fe^{3+}(Al,Si)_2O_7$ by electron microprobe analysis and X-ray diffraction (Coheur, 1969, Hancart *et al.*, 1967).

Malysheva and Batyrev (1970) considered this phase to be of an entirely different silicate class. Again using XRD and EPMA they found it to be a pyroxene of diopside–hedenbergite composition. Dyson and Juckes (1972) suggested a silicon-deficient clinopyroxene with the formula:

$$Ca_{1.14}Fe^{3+}_{0.86}(Fe^{3+}_{0.32}Al_{0.60}Si_{1.08})O_6$$

and proposed a *C*-face centred monoclinic cell; *a* 9.840, *b* 8.825, *c* 5.398 Å; β 105° 40′.

The fact that this remarkably high degree of Si replacement in the chain structure of pyroxene has passed without comment in the literature is very surprising, particularly since much of the replacement is by ferric ion. Subsilic clinopyroxene structures containing substantial amounts of trivalent cations, specifically Al^{3+}, are known. Dowty and Clarke (1973) report the clinopyroxene fassaite from the Allende meteorite which shows a high degree of Al for Si replacement in the silicate chain giving an average structural unit $(Al_{0.74}Si_{1.26})O_6$. This type of replacement can be expected since the Al^{3+} ion is isoelectronic with Si^{4+}, both adopting a tetrahedral arrangement of sp^3 hybridized bonding orbitals. The d^5 electronic configuration of Fe^{3+} cannot mimic silicon in the Si–O bond of the

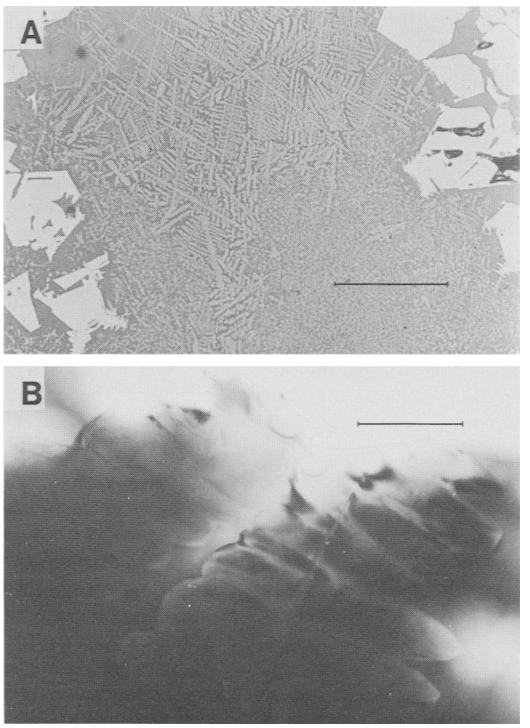

FIG. 4. The pyroxene-like mineral. (A) Reflected-light micrograph of the dendritic pyroxene set in a partially devitrified glass pool, surrounded by euhedral crystals of magnetite. Scale bar 0.1 mm. (B) TEM micrograph showing disc-shaped crystallites of pyroxene stacked in columns. Scale bar 1 μm.

silicate chain. Replacement of silicon by iron would fundamentally alter the nature of the SiO_4 unit and it seems unlikely that the chain silicate structure characteristic of pyroxenes could be maintained with any great degree of iron substitution.

It is possible that the Fe present in previous pyroxene-like analyses may have come from the presence of a co-precipitation of iron oxides finely dispersed amongst the dendritic mineral and beyond the resolution of the electron microprobe. The analytical TEM with its finer resolution is an ideal tool to address this question.

In the TEM the dendritic phase appeared as disc-shaped crystallites stacked in columns on their long edge (Fig. 4B). Even at high magnification and with a small analysis spot, there was no evidence of an intimate co-precipitation of iron oxide. Analyses of a large number of single discs revealed very little variation, the average analysis in Table 3 gives a mineral formula:

$$Ca_{1.02}Fe^{3+}_{0.83}(Fe^{3+}_{0.56}Al_{0.35}Si_{1.09})O_6.$$

Eleven different zones were recorded in selected-area diffraction patterns, all of which were consistent with the monoclinic unit cell of Dyson and Juckes (1972). Two zones were recorded containing the *h*00 reflections, both showing the absence of *h*-odd reflections. No diffraction pattern was recorded with the 0*k*0 reflections, but a single pattern with 00*l* reflections showed no systematic absences. This supports the *C*2/*c* symmetry reported by Dyson and Juckes.

This evidence indicates that a clinopyroxene unit cell is a good description of the crystallography of the dendritic phase in sinter. The *c*-axis of the unit cell, a measure of the repeat unit in the silicate chain, is rather long for a pyroxene. If there is a replacement of as much as half of the Si by Fe and Al, an expansion of the silicate repeat unit would be expected. However, although the data seem to confirm the silicon-deficient pyroxene, the novelty of such a highly iron-substituted silicate chain suggests it would be prudent to obtain a full single-crystal structural analysis.

The iron oxide minerals

Three oxides of iron commonly occur in sinter: magnetite, hematite and wüstite. Conditions on the sinter strand usually favour the reduction of hematite to magnetite with little further reduction to wüstite. However, due to the heterogeneous nature of sinter, the oxygen partial pressure may be such that hematite or wüstite may precipitate in some places. During the forced cooling of the sinter there is some solid-state oxidation of magnetite back to hematite (seen clearly in Fig. 1B).

In the analytical TEM, hematite invariably appeared as polycrystalline areas of very small grain size (of the order of microns). Diffraction from these areas gave ring patterns with even the smallest diffraction aperture, the ring spacings confirming hematite. Analysis of these areas proved them to be almost pure iron oxide with less than 2 wt. % of other oxides, chiefly Al_2O_3 and SiO_2.

Magnetite usually appeared as large crystals of uniform contrast, free from inclusions or alterations. Occasional grains appeared highly faulted; Ahsan *et al.* (1983) has shown these fault planes to be the (111) planes of magnetite. Analyses showed a wide range of substitution with up to about 11 wt. % iron oxide replaced by Al_2O_3, CaO, SiO_2 and MgO. Continuous solid solution exists between magnetite and magnesioferrite, $MgFe_2O_4$, and magnetite and hercynite, $FeAl_2O_4$, above 858 °C (Deer *et al.*, 1962). It is probable then that the maximum values found, 2.3 wt. % MgO and 4.9 wt. % Al_2O_3, are limited by the availability of these oxides in the melt rather than by solid-solution constraints. Chemical analysis by XRF indicates that the sinters studied generally contained less than 3 wt. % Al_2O_3 and 2 wt. % MgO. Conversely, the sinter melt is rich in lime and silica and the observed limits of 2.5 wt. % in both CaO and SiO_2 are likely to be due to the solid-solution constraints. Phillips and Muan (1958) suggest that a limit of about 2.4 wt. % CaO may enter the magnetite structure.

Calcium ferrites

The calcium ferrites are an important component of the matrix, improving both the strength and reducibility of the sinter. Much of the previous work on calcium ferrites in sinter has been concerned with those crystallising in the ternary CaO–FeO–Fe_2O_3 (e.g. Hughes *et al.*, 1967). With the availability of electron-probe microanalysis techniques it became apparent that the sinter ferrites contained significant amounts of Si and Al. Hancart *et al.* (1967) and Coheur (1969) called this phase silico-ferrite of Ca and Al or SFCA.

In the analytical TEM, it was clear that all the ferrites contained sufficient Al and Si to be of the SFCA type. No ferrites were found of purely Ca and Fe. Table 3 shows the average analysis; Fe is given in the ferric state since the total FeO content of sinter (from wet chemical techniques) is usually accounted for by the magnetite, wüstite and Fe–Ca orthosilicate, and most ferrites are reported as largely ferric (Hughes *et al.*, 1967). Two characteristics of SFCA analyses were noticed: no ferrites were found with less than about 3 wt. % Al_2O_3, and the ratio Ca : Si was consistently about 2 : 1. This

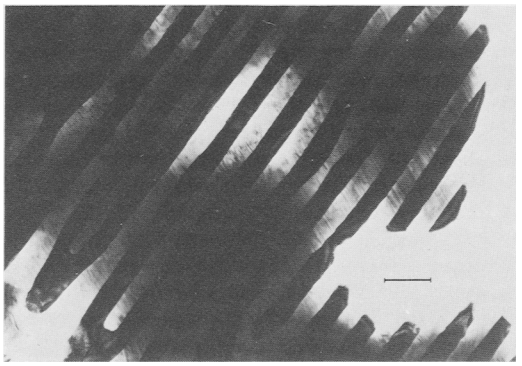

FIG. 5. TEM micrograph of magnetite (dark bands) and bredigite co-precipitated in a eutectic phase relationship. Scale bar 1 μm.

suggests that the SFCA may be an iron oxide with a coupled substitution of Ca and Si whose crystallisation is stabilised by a minimum level of Al. Some examples of low-alumina, self-fluxed sinters were abnormally deficient of SFCA and showed areas of the matrix abundant in a material with the characteristic 'lacy' texture. In the ATEM this proved to be a co-precipitation of iron oxide and iron-rich dicalcium silicate with an apparent eutectic phase-relationship (Fig. 5). Analyses showed CaO and SiO_2 in the oxide to be approaching the limit previously noted for magnetite, while the 10–15% iron oxide in the calcium silicate suggested, from earlier evidence, that the silicate should have the bredigite structure. Diffraction patterns obtained from the eutectic confirmed both magnetite and bredigite.

The SFCA appeared as twinned crystals with only one twin plane showing in any single grain (Fig. 6A). Lattice images showed the twinning to be on a very fine scale, of the order of a few nanometres. Ahsan *et al.* (1983) suggested that the unit cell may be related to the magnetite cell and that the twinning of SFCA is normal to the ⟨110⟩ crystallographic direction in magnetite.

In the TEM it is possible to rotate the SFCA crystal around the twin-plane normal to obtain a series of diffraction patterns and lattice images, each containing the prominent twin plane (an example is shown in Fig. 6A and B). Mulvaney (1984) showed how it is possible to deduce from this series of patterns a *C*-face centred monoclinic cell; *a* 9.79, *b* 15.08, *c* 5.30 Å; *β* 100° 01′ which bears a superlattice relationship to the magnetite unit cell:

$$(100)_{SFCA} \parallel (\bar{3}32)_M$$
$$(010)_{SFCA} \parallel (110)_M$$
$$(001)_{SFCA} \parallel (1\bar{1}2)_M$$

However, this gives the twin plane as the $(010)_{SFCA}$ plane, implying that this cell must be incorrect, because the (010) plane is a mirror plane in the monoclinic lattice.

Reworking the diffraction data gives another *C*-face centred monoclinic cell; *a* 15.70, *b* 9.70, *c* 8.48 Å; *β* 105° 30′. This cell has the (100) plane as the twin plane. Fig. 6B shows a diffraction pattern indexed on this cell.

The structure of SFCA and its relationship to magnetite remains unclear. SFCA might be similar to the ternary $Ca(Al_2Fe_4)O_{10}$ described by Lister and Glasser (1967), which they expected to occur in sintered iron oxide preparations made from aluminous ores. Mulvaney (1984) showed that SFCA and this ternary have similar X-ray diffraction spacings and intensities. The cell given by Lister and Glasser is *C*-face centred monoclinic; *a* 9.90, *b* 14.93, *c* 5.28 Å; *β* 101°. This bears a close resemblance to the earlier, discredited, cell proposed by Mulvaney (1984). Lister and Glasser remarked that the cell they give does not account for some of the weaker reflections obtained from the ternary phase, and therefore, the true cell may be different to the one they proposed.

The average composition of the SFCA samples found in sinter (Table 3) would fall into the solid-solution range of the ternary found by Lister and Glasser (1967). (In Table 3, the mineral formula for SFCA is based on 40 oxygens, the number of oxygens per unit cell given by Lister and Glasser.) It may prove beneficial to investigate the effect of adding silica to their ternary mixtures to determine the relationship between SFCA and $Ca(Al_2Fe_4)O_{10}$.

Summary

Earlier studies of iron ore sinters have been unable to characterise the detailed mineralogy because of the fine grain size of some of the phases. The use of modern analytical TEM techniques overcomes this limitation and new information on the mineralogy has emerged.

1. The essential constituents of the microtexture of basic sinter are relict and exsolved iron oxides bound in a matrix of SFCA (a complex calcium ferrite), calcium orthosilicate and glass.

2. Calcium orthosilicate is co-precipitated with SFCA. It is not, as earlier described, the single phase larnite. There is a range of Fe for Ca replacement in the basic Ca_2SiO_4 unit and three crystallographic forms were recognised which depend on the degree of Fe substitution. With little Fe substitution, that is in the range Ca_2SiO_4 to $Ca_{1.85}Fe_{0.15}SiO_4$, the structure is that of the medium-low temperature form of calcium ortho-

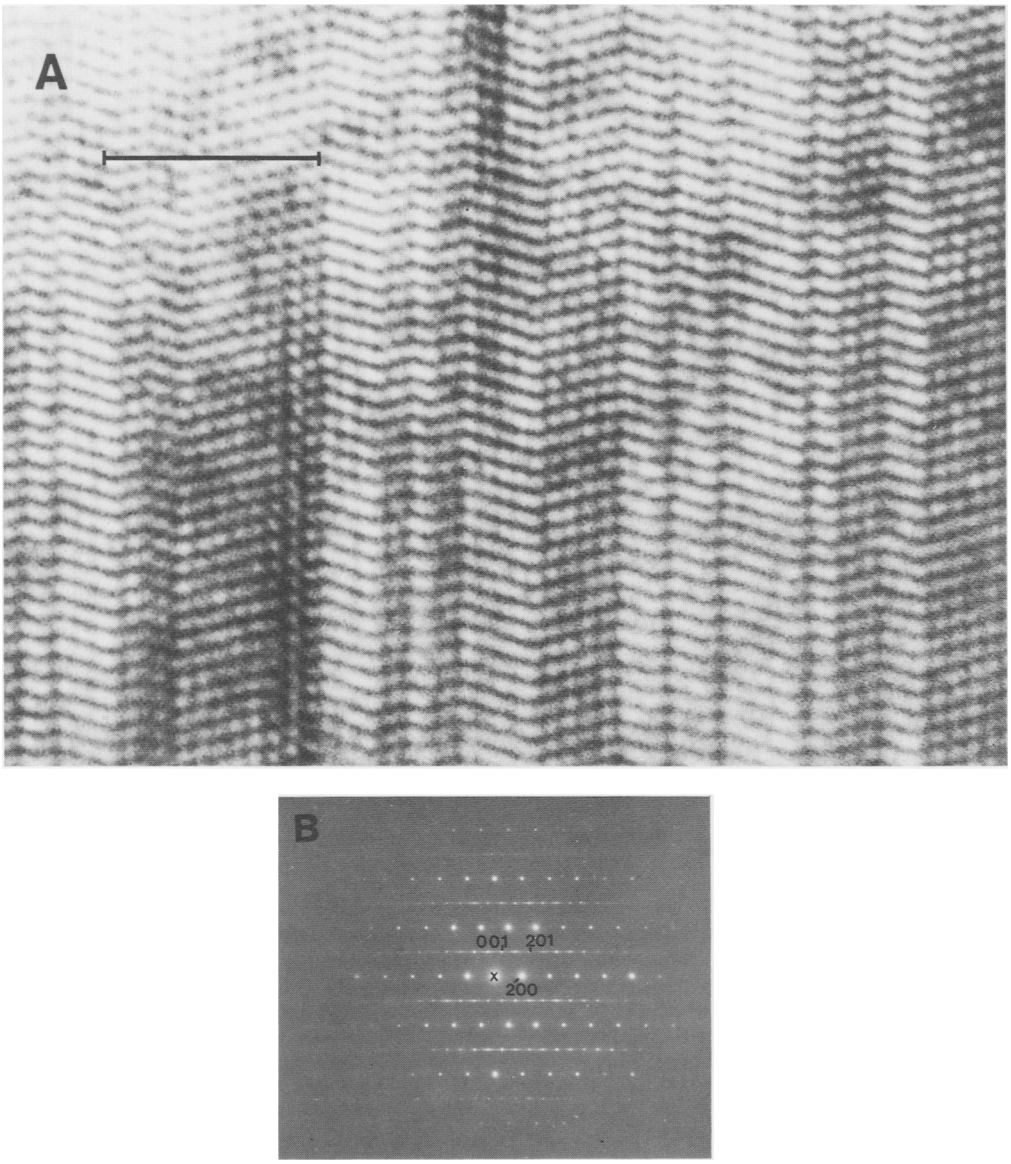

FIG. 6. TEM micrograph and electron diffraction pattern taken from the same area of an SFCA crystal, reproduced here in a consistent orientation. (A) The lattice image shows extensive twinning on a plane parallel to the monoclinic (100) plane. Scale bar 10 nm. (B) The [010] zone of SFCA. Indexing is based on the proposed *C*-face centred monoclinic cell: *a* 15.70, *b* 9.70, *c* 8.48 Å; β 105° 30′. The twinning is clear in this diffraction pattern.

silicate, β-Ca_2SiO_4 or larnite: monoclinic; *a* 5.507, *b* 6.754, *c* 9.317 Å; β 94° 37′. Increased Fe, in the range $Ca_{1.85}Fe_{0.15}SiO_4$ to $Ca_{1.6}Fe_{0.4}SiO_4$, gave the medium–high temperature form of calcium orthosilicate, bredigite or α'-Ca_2SiO_4, with an orthorhombic unit cell: *a* 10.91, *b* 18.41, *c* 6.76 Å. Fe substitution above this level, and to a possible limit of about $Ca_{1.5}Fe_{0.5}SiO_4$, gave a crystallographic form which was not recognisable as a polymorph of calcium orthosilicate. An orthorhombic unit cell was deduced for this phase: *a* 5.32, *b* 6.81, *c* 9.17 Å.

3. A dendritic alumino-iron silicate which precipitates from the glass has been described by Dyson and Juckes (1972) as a subsilic clinopyroxene. The pyroxene shows little compositional variability and has a mineral formula: $Ca_{1.02}Fe^{3+}_{0.83}(Fe^{3+}_{0.56}Al_{0.35}Si_{1.09})O_6$. The degree of Fe^{3+} and Al^{3+} substitution in the silicate chain implied by this formula makes this one of the most silicon-deficient clinopyroxenes reported. There is some doubt about the stability of the silicate chain with more than a quarter of the Si replaced by Fe^{3+}, but the evidence here tends to support the identification of this phase as a clinopyroxene. Diffraction patterns are consistent with a clinopyroxene-like, *C*-face centred monoclinic cell: *a* 9.840, *b* 8.825, *c* 5.398 Å; β 105° 40′.

4. Of the two oxides of iron recognised in the TEM, hematite tends to be virtually pure iron oxide while magnetite contains up to 11 wt. % Al_2O_3, CaO, SiO_2 and MgO.

5. The main matrix phase binding iron oxide grains in super-fluxed sinter is a complex calcium-ferrite known as SFCA (silico-ferrite of calcium and aluminium). Its composition is variable, but it is essentially a ferric oxide with a minimum of about 3 wt. % Al_2O_3 and contains 20 wt. % CaO and SiO_2, with a Ca : Si ion ratio of about 2 : 1. It has a *C*-face centred monoclinic cell: *a* 15.70, *b* 9.70, *c* 8.48 Å; β 105° 30′, and is extensively twinned parallel to the (100) plane. This phase may be related to the ternary $Ca(Al_2Fe_4)O_{10}$ described by Lister and Glasser (1967).

Acknowledgements

I am grateful to British Steel Corporation, Scunthorpe Division for supplying the sinter specimens and in particular to Dr D. Haynes. I thank Dr J. A. Whiteman of the Metallurgy Department and Professor C. D. Curtis of the Geology Department, Sheffield University, for their continuous enthusiastic encouragement. This work was undertaken while I was in receipt of an SERC CASE award.

References

Ahsan, S. N., Mukherjee, T., and Whiteman, J. A. (1983) *Ironmaking and Steelmaking*, **10**, 54–65.

Bowen, N. L., Schairer, J. F., and Posnjak, E. (1933) *Am. J. Sci.* **25**, 273–97.

Bredig, M. A. (1950) *J. Am. Ceram. Soc.* **33**, 188–92.

Bridge, T. E. (1966) *Am. Mineral.* **51**, 1766–74.

Cliff, G. and Lorimer, G. W. (1975) *J. Microscopy*, **103**, 203–7.

Coheur, P. (1969) *J. Iron Steel Inst.* **207**, 1291–7.

Deer, W. A., Howie, R. A., and Zussman, J. (1962) *Rock Forming Minerals*, **3**, Longman, London.

Dowty, E. and Clarke, J. R. (1973) *Am. Mineral.* **58**, 230–42.

Dyson, D. J. and Juckes, L. M. (1972) *Mineral. Mag.* **38**, 872–7.

Hancart, J., Leroy, V., and Bragard, A. (1967) *CNRM Metall. Rev.* **11**, 3–7.

Hughes, H., Roos, P., and Goldring, D. C. (1967) *Mineral. Mag.* **36**, 280–91.

Ireland, B. J. (1982) *Transmission electron microscopy of authigenic clay minerals.* Unpubl. PhD thesis, University of Sheffield.

Lister, D. H. and Glasser, F. P. (1967) *Trans. Brit. Ceram. Soc.* **66**, 293–305.

Malysheva, T. Y. and Batyrev, V. A. (1970) *Russ. Met. (Metally).* **3**, 8–11.

Mazanek, E. and Jasienska, S. (1968) *J. Iron Steel Inst.* **206**, 1104–9.

McBriar, E. M., Johnson, W., and Davies, W. (1954) Ibid. **177**, 316–23.

Midgely, C. M. (1952) *Acta Crystallogr.* **5**, 307–12.

Mulvaney, R. (1984) *The chemistry and mineralogy of iron ore sinters.* Unpubl. PhD thesis, University of Sheffield.

Nyquist, O. (1962) *Jernkont. Annlr*, **146**, 81–145.

Phillips, B. and Muan, A. (1958) *J. Am. Ceram. Soc.* **41**, 445–54.

Rankin, G. A. and Wright, F. E. (1915) *Am. J. Sci.* **39**, 1–79.

Scott, P. W., Critchley, S. R., and Wilkinson, F. C. F. (1986) *Mineral. Mag.* **50**, 141–7.

Tilley, C. E. and Vincent, H. C. G. (1948) Ibid. **28**, 255–71.

Wyderko, M. and Mazanek, E. (1968) Ibid. **36**, 955–61.

Zerfoss, S. and Davis, H. M. (1943) *J. Am. Ceram. Soc.* **26**, 302–7.

[*Revised manuscript received 25 August 1986*]